Journal of Dental Sciences 19 (2024) S70—S80

Available online at www.sciencedirect.com

ScienceDirect

journal homepage: www.e-jds.com

Original Article

Creating an extracellular matrix-like three-dimension structure to enhance the corrosion resistance and biological responses of titanium implants

Ying-Sui Sun [a*], Her-Hsiung Huang [b,c,d,e], Yi-Hsuan Tsai [f], Yu-Lin Kuo [g], Jyh-Wei Lee [h], Yun-Jung Lee [a], Thu Ya Linn [i], Peng Chen [j]

[a] School of Dental Technology, College of Oral Medicine, Taipei Medical University, Taipei, Taiwan
[b] Department of Dentistry, National Yang Ming Chiao Tung University, Taipei, Taiwan
[c] Department of Bioinformatics and Medical Engineering, Asia University, Taichung, Taiwan
[d] Department of Medical Research, China Medical University Hospital, China Medical University, Taichung, Taiwan
[e] School of Dentistry, Kaohsiung Medical University, Kaohsiung, Taiwan
[f] Institute of Oral Biology, School of Dentistry Graduate, National Taiwan University, Taipei, Taiwan
[g] Department of Mechanical Engineering, National Taiwan University of Science and Technology, Taipei, Taiwan
[h] Department of Materials Engineering, Ming Chi University of Technology, New Taipei, Taiwan
[i] School of Dentistry, College of Oral Medicine, Taipei Medical University, Taipei, Taiwan
[j] Liaison Center for Innovative Dentistry, Graduate School of Dentistry, Tohoku University, Sendai, Japan

Received 31 July 2024; Final revision received 15 September 2024
Available online 24 September 2024

KEYWORDS
Titanium implant;
Surface treatment;
Porous oxide layer;
Corrosion resistance;
Biological response

Abstract *Background/purpose:* Titanium (Ti) is extensively used in dental and orthopedic implants due to its excellent mechanical properties. However, its smooth and biologically inert surface does not support the ingrowth of new bone, and Ti ions may have adverse biological effects. The purpose is to improve the corrosion resistance of titanium and create a 3D structured coating to enhance osseointegration through a very simple and fast surface treatment. *Materials and methods:* This study investigated the use of sandblasting, acid etching, and NaOH leaching to produce porous Ti implants with enhanced biological activity and corrosion resistance.

* Corresponding author. School of Dental Technology, College of Oral Medicine, Taipei Medical University, No. 250, Wu-Hsing Street, Xinyi District, Taipei, 110, Taiwan.
E-mail address: yingsuisun@tmu.edu.tw (Y.-S. Sun).

https://doi.org/10.1016/j.jds.2024.09.007
1991-7902/© 2024 Association for Dental Sciences of the Republic of China. Publishing services by Elsevier B.V. This is an open access article under the CC BY-NC-ND license (http://creativecommons.org/licenses/by-nc-nd/4.0/).

Results: These surface modifications generated a mixed oxide layer resembling the extracellular matrix (ECM), consisting of a dense amorphous TiO2 inner layer (50—100 nm thick) and a TiO2 outer layer with interconnected pores (pore size 50—500 nm; 150—200 nm thick). The inner layer significantly improved corrosion resistance, while the hydrophilic outer layer, with its porous structure, facilitated protein albumin adsorption and promoted the attachment, proliferation, and mineralization of human bone marrow mesenchymal stem cells.
Conclusion: The combined surface treatment approach of sandblasting, acid etching, and NaOH leaching offers a comprehensive solution to the challenges associated with titanium implants' biological inertness and corrosion susceptibility. By enhancing both the biological activity and corrosion resistance of Ti surfaces, this protocol holds significant promise for improving dental and orthopedic implants' success rates and longevity. Future studies should focus on in vivo assessments and long-term clinical trials to further validate these findings and explore the potential for widespread clinical adoption.
© 2024 Association for Dental Sciences of the Republic of China. Publishing services by Elsevier B.V. This is an open access article under the CC BY-NC-ND license (http://creativecommons.org/licenses/by-nc-nd/4.0/).

Introduction

The biocompatibility of the titanium (Ti) implants/restorations currently used in dentistry depends on the proportions of elements in the alloy and a continuous titanium dioxide (TiO_2) surface layer. The release of small quantities of ions from passivated surfaces does not generally damage the implant surface; however, there is evidence that under oral conditions (mastication and pH of 5.2—7.8), the TiO_2 layer can deteriorate or corrode.[1,2] The resulting release of ions into the oral cavity can cause allergic reactions in oral tissues and even lead to implant failure by preventing the implant surface from re-bonding with surrounding bone.[3] Numerous studies have addressed the cytotoxic responses and antibacterial effects of surface-treated Ti and Ti alloys.[4,5] Typical reactions to implant erosion include bone loss due to inflammation,[6,7] systemic side effects due to allergic reactions to Ti,[8] and yellow nail syndrome.[4,9]

Osteointegration is a dynamic and complex biological process governed by the absorption of proteins onto the implant surface immediately following its insertion.[10] This process, assuming the integration of the implant into the bone, establishes a direct connection to the bone, resulting in a secure anchorage.[11] Osteointegration's success is influenced by factors such as surface topography, chemical composition, hydrophilicity, and surface roughness. It is also closely associated with the processes of osteoconduction, osteoinduction, and osteogenesis.[10—12] Furthermore, the topography of the implant surface plays a critical role in determining the cytoskeletal organization of primary osteoblast cells, thereby influencing their functionality in both *in vitro* and in vivo settings.[13]

Several surface modifications have been devised to enhance the biocompatibility and performance of Ti and its alloys in implant applications. The primary aim of most surface modification techniques is to promote osseointegration of the implant with the surrounding new bone and improve corrosion resistance in physiological environments. On Ti-6Al-4V or β-Ti alloy implants, this often involves the growth of passive protective layers consisting mainly of TiO_2. The methods used for the creation of these layers include electrochemical passivation, thermal oxidation, and plasma electrolytic oxidation.[14] Osseointegration involves a series of processes, including cell attachment, proliferation, differentiation, and new bone mineralization. The success of osseointegration depends largely on the properties of the implant surface, such as roughness, porosity, and topography.[15] One common approach to creating a suitable surface involves the use of sandblasting in conjunction with acid etching. Note that some surface treatment methods affect the surface structure and roughness, whereas others affect the chemical properties.[16] Moreover, hydrophilicity of the material surface is also a key issue that determines the biocompatibility of implant surfaces, which will affect many cell responses.[17—20]

The core cellular behaviors of migration, adhesion, proliferation, and differentiation are profoundly influenced by the structural composition of the extracellular matrix (ECM), which is in turn shaped by the surrounding physiological environment.[21,22] In fact, cellular behavior can be altered simply by changing the growth environment. Cell migration relies on physical contact to guide anterograde alignment and the spreading of cells on the material surface. In one study, aligning cells in the direction of grooves (150 nm—4.0 μm) was shown to facilitate cell proliferation.[22] In another study, aligning osteoblasts along distinct grooves (75 nm wide and 50 nm deep) promoted the self-alignment behavior of cell pseudopodia.[23] The adhesion and proliferation of fibroblasts and mesenchymal cells can also be affected by nanoscale surface structures.[24] Overall, rough surfaces are better suited to osseointegration than are polished surfaces.

In the field of dental biomaterials, significant advancements have been made in improving osteointegration through a multifaceted approach. This includes the deployment of innovative materials, the application of advanced surface modification techniques such as coatings and topological enhancements, and the employment of composite materials designed to foster synergistic interactions among their components. These strategies not only bolster the integration of implants with surrounding

bone tissue but also optimize the bone regeneration process post-implantation, thereby enhancing patient recovery outcomes and the long-term stability of the implants. By leveraging these sophisticated surface treatment technologies, it's possible to finely tune the chemical and physical properties of implant surfaces at the micro-level, which further improves their biocompatibility and osteointegration capabilities with human bone tissue.[25]

The objective of this study was to modify the surface of Ti implants using sandblasting in conjunction with acid etching and NaOH leaching. Our ultimate aim was to improve corrosion resistance and create 3D surface structures conducive to the formation of ECM-like filaments with an overlapping morphology to enhance osseointegration.

Materials and methods

Sample preparation

This study investigated the use of sandblasting, acid etching, and NaOH leaching to produce porous Ti implants with enhanced biological activity and corrosion resistance. Disc samples of commercial grade 4 Ti (15 mm diameter, 1.5 mm thickness; UMAT, Hsinchu, Taiwan) were subjected to surface grinding using #1200 Sci paper. Some of the Ti samples were held in reserve (i.e., without further treatment) as a control group (referred to as T). The element contribution (%) of the Ti sample was as follows: Fe (0.3), C (0.06), O (0.3–0.4), H (0.01), Si (0.005), N (0.04), Ti (nil).

Some of the T discs underwent sandblasting (S) using 120 μm alumina grit to form TS samples. Some of the TS disks were then etched in an acid bath of HNO_3/HF (Merck KGaA, Darmstadt, Germany) to form TSA_F samples (where F refers to HF) or HCl/H_2SO_4 (Merck KGaA) to form TSA_S samples (where S refers to H_2SO_4). Note that the former acid solution comprised 50% HF: 70% HNO_3: ddH_2O = 1:9:40, whereas the latter acid solution comprised 5 mol/L HCl: 9 mL/L H_2SO_4 = 1:1. Acid treatment was performed in Petri dishes under a chemical hood at 37 °C for 24 h.

Some of the TS, TSA_F, and TSA_S samples were then soaked in a 5M NaOH alkaline (A) solution to form TSA, TSA_FA and TSA_SA samples, respectively. Alkaline treatment involved immersing the disks in 5M NaOH solution (~100 mL) at room temperature. The disks were subsequently cleaned using deionized H_2O under sonication for 10 min, followed by forced air drying in an oven at 60 °C overnight (~12 h). This resulted in a total of eight groups for analysis: T, TS, TSA_F, $TiSA_S$, TiA, TiSA, $TiSA_FA$, and $TiSA_SA$.

Surface characterization

The surface topography and 3D structures were characterized using a field emission scanning electron microscope equipped with an energy-dispersive X-ray spectroscope (FE-SEM/EDS; JEOL 7900F, JEOL Ltd, Tokyo, Japan), operating at a voltage of 5 kV, after coating the sample surfaces with platinum to a thickness of roughly 6 nm.

Cross-sections of the three-dimensional surface structures were examined using Dual Beam FIB (FEI Quanta 3D FEG; FEI company, Hillsboro, OR, USA). Surface roughness (Ra) was calculated using a surface profiler (α-step ET200, Kosaka Laboratory Ltd, Tokyo, Japan). The thickness of the oxide layer was determined using an X-ray photoelectron spectroscope (XPS; ULVAC-PHI, PHI 5000 VersaProbe, ULVAC- PHI Inc, Kanagawa, Japan) with a pass energy of 58.7 eV and C60 depth profiling. The surface crystalline phase composition was characterized using X-ray diffraction (XRD; Bruker D8 DISCOVER, Billerica, MA, USA). Surface wettability was estimated from contact angle measurements obtained using a contact angle goniometer (MagicDroplet 100SL, Sindatek Instruments Ltd., Taipei, Taiwan).

Surface bioactivity testing involved soaking samples in simulated body fluid solution for 7 days with the solution refreshed at intervals of 48 h. After the 7-day soaking period, the samples were dried and subjected to FE-SEM/EDS (JEOL Ltd) analysis to observe the surface morphology and composition of deposits on sample surfaces.

Corrosion resistance

An electrochemical workstation (Jiehan 5000, Jiehan Technology Co., Taichung, Taiwan) was used to obtain potentiodynamic polarization curves were obtained using the sample as a working electrode, a saturated calomel electrode (SCE) as a reference electrode, and a platinum sheet as a counter electrode from −0.5 V to +2 V (vs. SCE) with simulated blood plasma (SBP) used as the electrolyte (pH 7.4, 37 °C).

Responses of human bone marrow mesenchymal stem cells

GFP-labeled human bone marrow mesenchymal stem cells (hMSCs) were cultured on test samples at a density of 5×10^4 cells/disc. After 3 h, the number of cells adhering to the test samples was assessed *in situ* using a fluorescence optical microscope. In parallel tests, cells adhering to test samples were sequentially fixed, dehydrated, and dried using a critical point dryer. Samples were then coated with a thin film of platinum to observe the morphology of adhered cells via FE-SEM analysis.

Cell proliferation on test samples was characterized via alamarBlue® test assays (Biosource International, Lewisville, TX, USA), which involved seeding hMSCs (1×10^4 cells/disc) on test samples in 24-well plates. After each culture period (1, 3, and 5 d), the cell-seeded samples were incubated in culture medium with 10% alamarBlue® reagent under an atmosphere of 5% CO_2 at 37 °C for 6 h. The culture medium was then transferred to 96-well plates to quantify the absorbance spectrophotometrically using a microplate photometer at wavelengths of 570 and 600 nm. Non-seeded 96-well plates were subjected to the same procedures to provide a blank control.

Cell mineralization on test samples was analyzed qualitatively and quantitatively based on the formation of calcium compounds using Alizarin red S (Sigma–Aldrich, St Louis, MO, USA) staining. hMSCs were cultured at a density of 10^4 cells/disc in normal culture medium for 1 day prior to immersion in an osteogenic medium containing DMEM supplemented with 50 μg/mL ascorbic acid, 10 mM β-

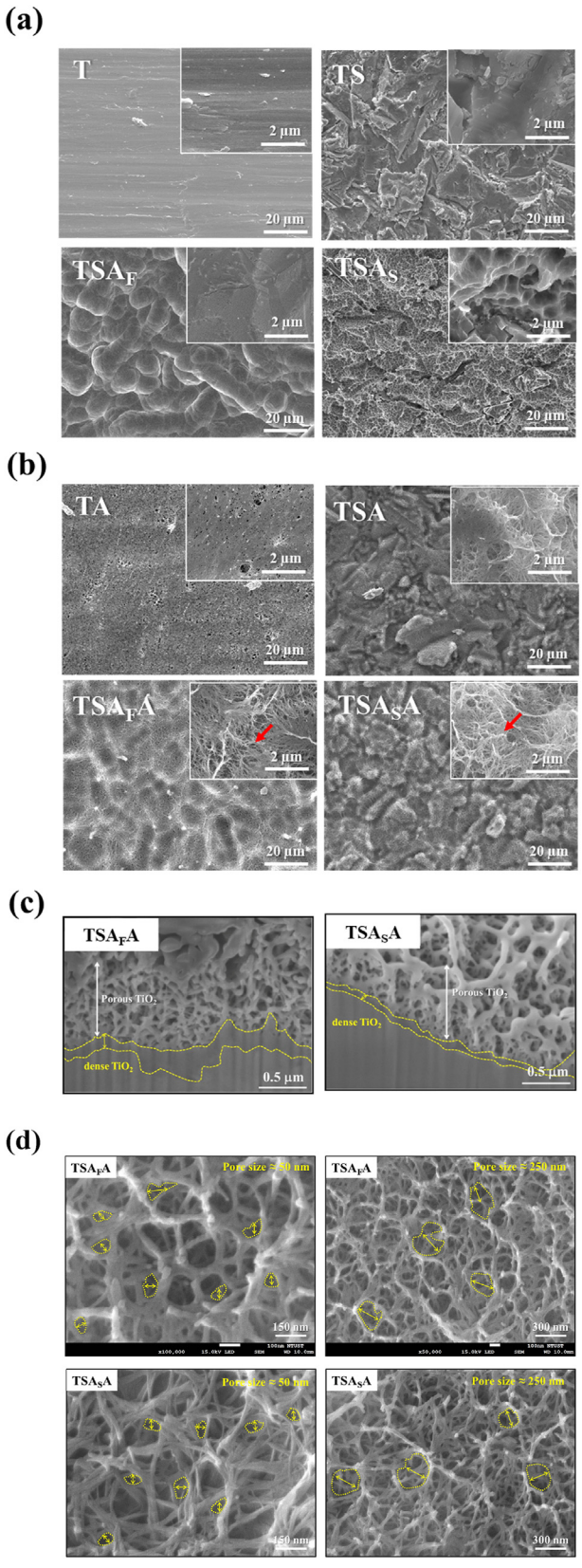

Figure 1 Field emission scanning electron microscopy images showing the surface morphology (top view) of samples (a) before acid treatment (T, TS) and after acid treatment (TSA$_F$, TSA$_S$); (b) after alkaline treatment; (c) cross-section images showing pore structure. (d) This is a high-magnification picture. It can be seen from the picture that the surface of the NaOH-treated material has a pore size structure of 50～250 nm. T: grade 4 Ti; TS: T discs underwent sandblasting; TSA$_F$: the TS disks were etched in an acid bath of HNO_3/HF; TSA$_S$: the TS disks were etched in an acid bath of HCl/H_2SO_4; TSA, TSA$_F$A and TSA$_S$A: the TS, TSA$_F$, and TSA$_S$ samples were soaked in NaOH.

glycerophosphate, and 10^{-8} M dexamethasone (all from Sigma–Aldrich). The osteogenic medium was changed every 48 h. After incubation for 7 or 14 d, cells were sequentially fixed and stained using Alizarin red S (2%) at room temperature for 20 min. Mineralization of the ECM-LIKE resulted in large deposits of calcium and phosphorus ions. The stained cells were immersed in cetylpyridinium chloride (CPC) and sodium phosphate at room temperature under shaking for 1 h. OD values were recorded using a microplate photometer at a wavelength of 540 nm, where higher OD values indicated more extensive cell mineralization. Note that the OD values of the blank groups (the same surface treatment without cell culture) were below 0.01 (nearly negligible) and were subtracted from the measured OD values of the corresponding test groups.

Statistical analysis

Five samples were obtained from each test group at each time point for each measurement, and all measurements were performed in triplicate. Experimental data are presented as mean ± standard deviation (SD). Student t-test was used to analyze the effects of surface treatment on surface roughness and cell responses, with the level of significance set at $\alpha = 0.05$.

Results

Surface characterization

In the current study, we focused on creating a surface topography that would promote osteocyte responses. As shown in the FE-SEM micrograph in Fig. 1, the size of the surface pores on all surface-treated samples ranged from a few nm to 100 nm. Note that this treatment resulted in morphology with surface features ranging in size from the nanometer to the sub-micrometer scales. The pore size distribution was approximately 50～250 nm and evenly distributed. The thickness of the 3D hole structure was approximately 600～800 nm. The thickness of the dense TiO_2 layer was approximately 500～200 nm (Fig. 1 (c)). The Ra results are shown in Fig. 2., T = 0.19; TS = 1.47; TSA$_F$ = 1.33; TSA$_F$A = 1.31; TSA$_S$ = 1.89; TSA$_S$A = 2.08. Relative to the titanium surface etched by hydrofluoric acid solution, the Ra value after sulfuric acid treatment larger.

As shown in Fig. 3, XPS analysis (O1s and Ti2p) revealed micron-scale pits on TSA$_F$ and TSA$_S$ samples. Acid treatment had a pronounced effect in promoting the formation of a surface oxide layer on TSA$_S$ samples but not on TSA$_F$ samples. NaOH treatment was shown to promote the formation of the surface oxide layer, particularly on TSA$_S$A samples.

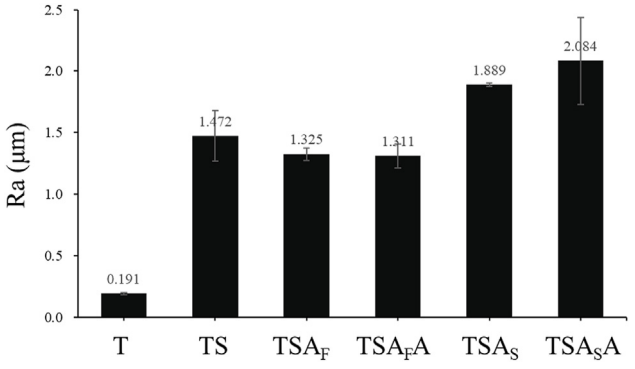

Figure 2 Surface roughness of all samples as indicated by α-step. T: grade 4 Ti; TS: T discs underwent sandblasting; TSA$_F$: the TS disks were etched in an acid bath of HNO_3/HF; TSA$_S$: the TS disks were etched in an acid bath of HCl/H_2SO_4; TSA, TSA$_F$A and TSA$_S$A: the TS, TSA$_F$, and TSA$_S$ samples were soaked in NaOH.

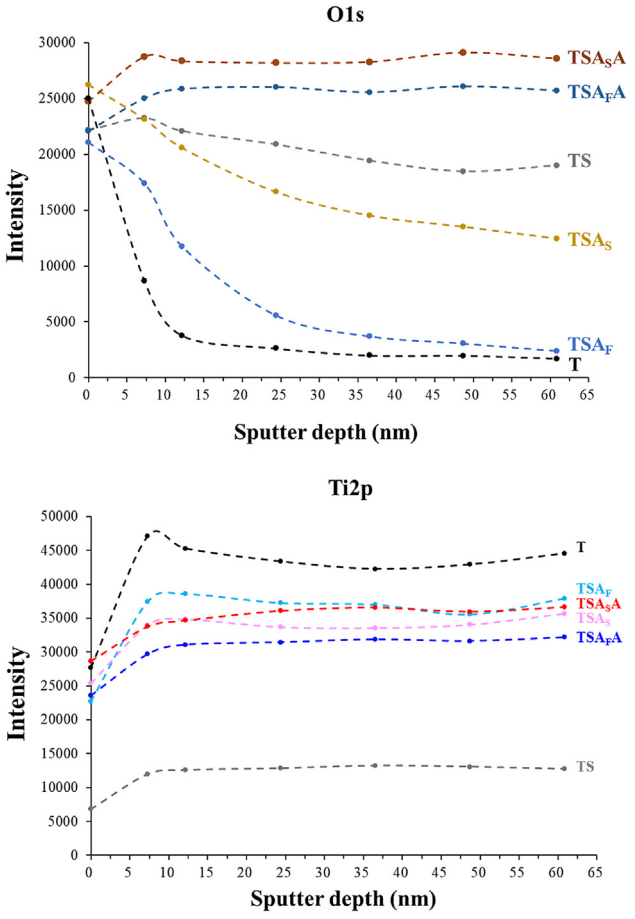

Figure 3 Element composition (O1s and Ti2p) of sample surfaces derived from X-ray photoelectron spectroscopy results. T: grade 4 Ti; TS: T discs underwent sandblasting; TSA$_F$: the TS disks were etched in an acid bath of HNO_3/HF; TSA$_S$: the TS disks were etched in an acid bath of HCl/H_2SO_4; TSA, TSA$_F$A and TSA$_S$A: the TS, TSA$_F$, and TSA$_S$ samples were soaked in NaOH.

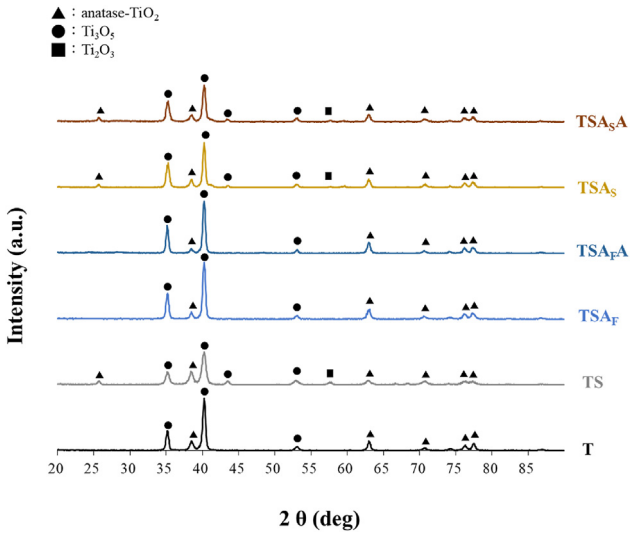

Figure 4 Crystallographic structure of sample surfaces based on X-ray diffraction analysis. T: grade 4 Ti; TS: T discs underwent sandblasting; TSA$_F$: the TS disks were etched in an acid bath of HNO_3/HF; TSA$_S$: the TS disks were etched in an acid bath of HCl/H_2SO_4; TSA, TSA$_F$A and TSA$_S$A: the TS, TSA$_F$, and TSA$_S$ samples were soaked in NaOH.

As shown in Fig. 4, anatase-TiO_2 ($2\theta = 25.5°$) and Ti_2O_3 ($2\theta = 57.5°$) were identified on Ti surfaces after sandblasting (TS group). On samples treated with HF acid (TSA$_F$), the anatase phase structure was not detectable. Samples treated with sulfuric acid retained the anatase phase (TSA$_S$). In other words, HCl/H_2SO_4 was more effective than HNO_3/HF in promoting the formation of the anatase phase. As shown in Fig. 5, the surfaces of TSAFA and TSASA samples were highly hydrophilic, as evidenced by water contact angles of 3.3 and 0°, respectively.

Corrosion resistance in simulated blood plasma

Fig. 6 presents potentiodynamic polarization curves of TSA$_F$A samples following immersion in SBP. All the samples presented passivated areas, regardless of whether they underwent acid-etching and/or alkaline immersion. As expected, the TSA$_S$A sample presented the highest I*pass* value, far exceeding (nearly double) that of T samples.

Table 1 lists all corrosion parameters derived from the polarization curves of samples after immersion in SBP. The E*corr* (vs. SCE) value of TSA$_S$A (−826 mV) was higher than that of T samples (−680 mV) and TSA$_S$ samples (−555 mV), indicating superior corrosion resistance. The I*corr* values of TSA$_F$A (0.92 μA/cm^2) and TSA$_S$A (0.136 μA/cm^2) were notably higher than that of Ti (0.0566 μA/cm^2). The I*pass* values of TSA$_S$ (8.27 μA/cm^2) and TSA$_S$A (12.07 μA/cm^2) were higher than those of T, whereas the values of TSA$_S$A were higher than those of TSA$_S$.

Responses of human bone marrow mesenchymal stem cells

The hMSCs cultures in the current study revealed that roughening the surfaces enhanced cell attachment and

	T	TS	TSA_F	TSA_FA	TSA_S	TSA_SA
ddH_2O (polar)	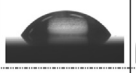					
Contact angle	58.67°	50.54°	108.24°	3.33°	138.63°	0°
CH_2I_2 (non-polar)						
Contact angle	37.21°	36.28°	54.88°	43.06°	115.07°	24.77°
Surface free energy (mN/m)	**53.67±2.58**	**58.47±1.29**	**31.54±2.19**	**75.90±3.74**	**4.22±0.95**	**79.28±3.88**

Figure 5 Surface wettability based on contact angle goniometer results. T: grade 4 Ti; TS: T discs underwent sandblasting; TSA_F: the TS disks were etched in an acid bath of HNO_3/HF; TSA_S: the TS disks were etched in an acid bath of HCl/H_2SO_4; TSA, TSA_FA and TSA_SA: the TS, TSA_F, and TSA_S samples were soaked in NaOH.

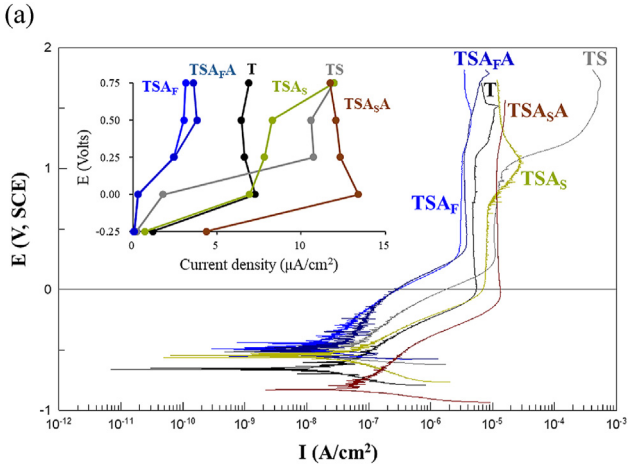

Figure 6 Corrosion resistance in simulated blood plasma based on potentiodynamic polarization curves. T: grade 4 Ti; TS: T discs underwent sandblasting; TSA_F: the TS disks were etched in an acid bath of HNO_3/HF; TSA_S: the TS disks were etched in an acid bath of HCl/H_2SO_4; TSA, TSA_FA and TSA_SA: the TS, TSA_F, and TSA_S samples were soaked in NaOH.

proliferation *in vitro* The FE-SEM micrographs in Fig. 7 revealed excellent cell adhesion to the alloy substrate with cell spreading and cell-to-cell interactions after incubating hMSCs cells in the presence of TSA_FA samples for 3 h.

Fig. 8 illustrates the proliferation of hMSCs on the test samples after culturing for five days. At days 1–3, pronounced cell proliferation was observed on NaOH-treated

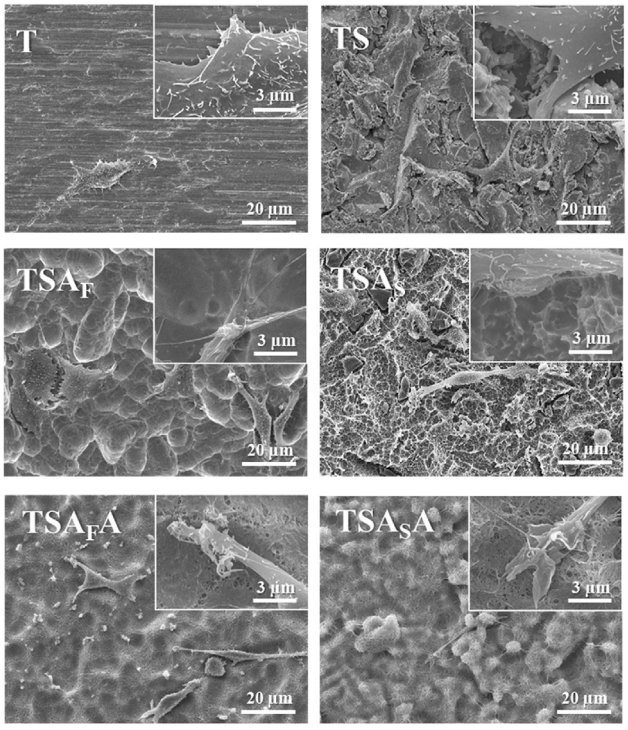

Figure 7 Field emission scanning electron microscopy images showing cell adhesion and filopodia spreading behavior (culture time: 3 h). T: grade 4 Ti; TS: T discs underwent sandblasting; TSA_F: the TS disks were etched in an acid bath of HNO_3/HF; TSA_S: the TS disks were etched in an acid bath of HCl/H_2SO_4; TSA, TSA_FA and TSA_SA: the TS, TSA_F, and TSA_S samples were soaked in NaOH.

Table 1 Quantitative data (E_{corr}, I_{corr}, Rp, and I_{pass}) and polarization curves of all groups subjected to corrosion resistance testing at 0.5 V.

	T	TS	TSA_F	TSA_FA	TSA_S	TSA_SA
E_{corr} (mV)	−680	−530	−493	−553	−555	−826
I_{corr} (μA/cm^2)	0.0566	0.0456	0.0351	0.92	0.0425	0.136
Rp (Ohms*cm^2)	4.61×10^5	5.72×10^5	7.44×10^5	2.83×10^4	6.13×10^5	1.92×10^5
I_{pass} at 0.5 V (μA/cm^2)	6.4365	10.59	3.03	3.8	8.27	12.07

T: grade 4 Ti; TS: T discs underwent sandblasting; TSA_F: The TS disks were etched in an acid bath of HNO_3/HF; TSA_S: The TS disks were etched in an acid bath of HCl/H_2SO_4; TSA, TSA_FA and TSA_SA: the TS, TSA_F, and TSA_S samples were soaked in NaOH.

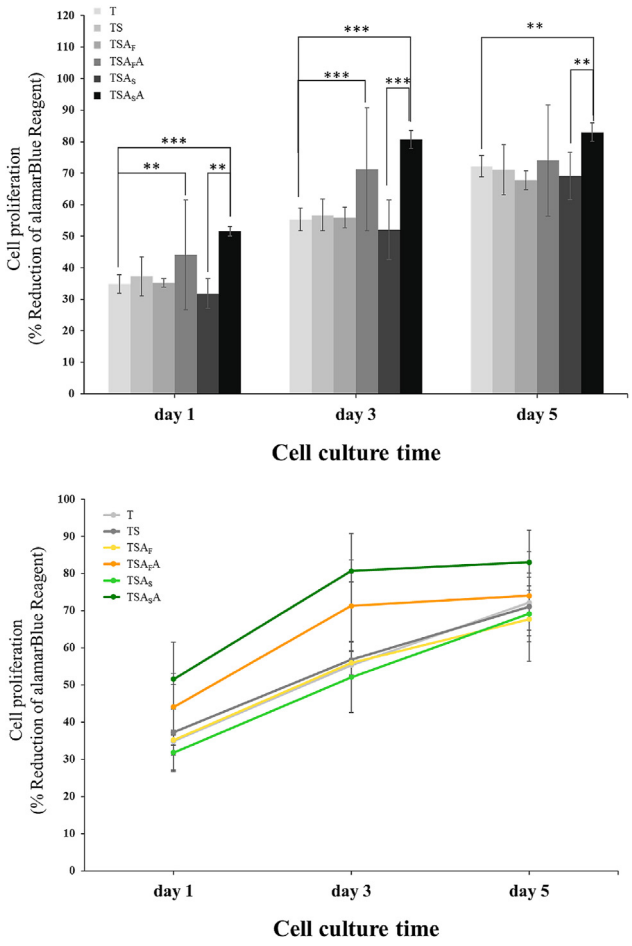

Figure 8 AlamarBlue staining results showing cell proliferation (a) among groups and (b) between groups. T: grade 4 Ti; TS: T discs underwent sandblasting; TSA$_F$: the TS disks were etched in an acid bath of HNO_3/HF; TSA$_S$: the TS disks were etched in an acid bath of HCl/H_2SO_4; TSA, TSA$_F$A and TSA$_S$A: the TS, TSA$_F$, and TSA$_S$ samples were soaked in NaOH. (*P*-value: *<0.05; **<0.01; ***<0.001).

samples (TSA$_F$A and TSA$_S$A). On day 1, the cell counts on TSA$_S$A samples was 1.5 times higher than on TSA$_S$ samples and 1.2 times higher than on TSA$_F$A samples. Note that the benefits of alkaline treatment accrued over time, as evidenced by cell count assays on days 3 and day 5.

Alizarin red S staining was used for the cell mineralization test to characterize the formation of calcium-rich surface deposits. Optical microscope analysis provided a qualitative indication of mineralized calcium deposits in pores at the nano-to sub-micro scale. As shown in Fig. 9, cell mineralization was more pronounced in acid-treated groups than in untreated samples at 7 and 14 days. Note that mineralization was particularly pronounced in TSA$_S$ samples (Fig. 9 (a)). The area affected by mineralization was quantified in terms of mean color intensity. Alizarin Red staining was more pronounced on samples that underwent alkaline treatment (TSA$_F$A and TSA$_S$A). We believe that this was due to the deposition of calcium in the nanopores and the incomplete dissolution of calcium ions in the pores during CPC treatment (Fig. 9 (b)). The formation of distinct calcium nodules on TSA$_S$ and TSA$_F$ surfaces revealed the effects of surface treatment on mineralization. The light staining on Ti controls indicated the deposition of very little calcium.

In vitro bioactivity

Moreover, we examined the *in vitro* bioactivity of implants after each surface treatment. As shown in Fig. 10, calcium and phosphorus ions appeared on the surface of the NaOH-treated material but not on untreated surfaces. Note that the calcium/phosphorus ratio did not vary considerably as a function of acid treatment: TSA$_F$A (Ca/P≈1.42) and TSA$_S$A (Ca/P≈1.36). Under a Ca/P ratio of 1.42, the composition was Cax(PO_4)y (amorphous calcium orthophosphate). Under a Ca/P ratio of 1.36, the composition was $Ca_8H_2(P0_4)_6$' $5H_20$ (octacalcium orthophosphate).

Discussion

Cellular responses depend largely on surface roughness. Researchers have recently recognized the benefits of tissue-like 3D microenvironments (e.g., 3D culture systems), which preserve the morphology of cells as well as their physiological, biochemical, and biomechanical functions.[18,19] In Fig. 1, the surface pore size is below 100 nm. Especially on the material surface of TSA$_F$A and TSA$_S$A, it can be observed that the pore size distribution on the surface of the material is approximately 50～250 nm and is evenly distributed. Moreover, the porosity structure of 50～250 nm is a 3D mixed structure (Fig. 1 (d)). However, NaOH has little effect on the roughness of the titanium surface. No matter in the TSA$_F$A or TSA$_S$A group, there is no significant difference in the Ra value of the titanium surface after NaOH treatment (Fig. 2). Observed from the cross section, the thickness of the 3D pore structure is approximately 600～800 nm. The thickness of the dense TiO_2 layer is approximately 500～200 nm.

It can be seen from the XPS results of O1s and Ti2p that acid treatment has a significant effect on promoting the formation of oxide layer on the surface of TSAS samples, but not on TSAF samples (surface treated with hydrofluoric acid solution). NaOH treatment has been shown to promote the formation of surface oxide layers, especially on TSAS samples (surfaces treated with sulfuric acid solution). The above discussion can be seen in Fig. 3.

Micron-sized pits were present on the TSAF and TSAS samples (Fig. 1(a)). It appears that the acid solution caused a chemical reaction with the titanium, causing holes in the surface to be etched. Subsequent immersion in NaOH solution promoted the formation of surface corrosion products, leading to the formation of a nanoporous oxide layer (Fig. 1(b)). The interconnected pores also lead to the formation of a coating surface with a 3D Ti-O structure (Fig. 1(c)). The presence of some titanium oxide products can be demonstrated by the data displayed by XPS analysis (Fig. 3).

According to Figs. 3 and 4, anatase-TiO_2 and Ti_2O_3 were identified on Ti sandblasting surfaces after. However, the anatase phase structure was not detectable on samples treated with HF acid. Samples treated with sulfuric acid

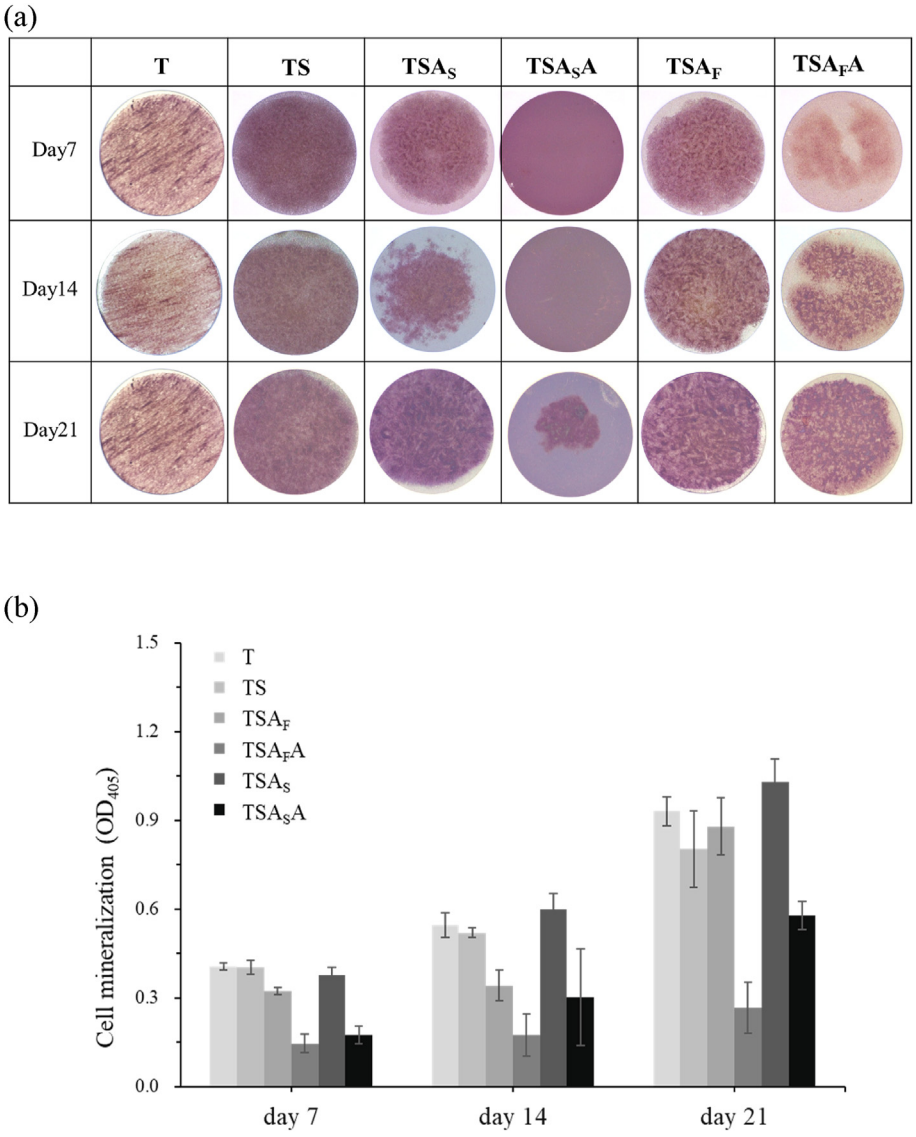

Figure 9 Cell differentiation results (Alizarin red) showing (a) qualitative and (b) quantitative outcomes at 7, 14 and 21 days. T: grade 4 Ti; TS: T discs underwent sandblasting; TSA_F: the TS disks were etched in an acid bath of HNO_3/HF; TSA_S: the TS disks were etched in an acid bath of HCl/H_2SO_4; TSA, TSA_FA and TSA_SA: the TS, TSA_F, and TSA_S samples were soaked in NaOH.

retained the anatase phase. In other words, HCl/H_2SO_4 was more effective than HNO_3/HF in promoting the formation of anatase phase.

According to specifications outlined by the American Society for Testing and Materials (D7334-08), a contact angle of 10—20° indicates good wetting behavior.[16] As shown in Fig. 5, the surfaces of TSA_FA and TSA_SA samples were highly hydrophilic, as evidenced by water contact angles of 3.3 and 0°, respectively. The grafting of OH^- functional groups on the surface of the NaOH-treated samples has previously been shown to increase surface hydrophilicity.[17] OH^- functional groups can also induce the adsorption of Ca^{+2} ions.

In the current study, we examined the *in vitro* bioactivity of implants after each surface treatment. As shown in Fig. 10, calcium and phosphorus ions appeared on the surface of the NaOH-treated material but not on untreated surfaces. Note that the calcium/phosphorus ratio did not vary considerably as a function of acid treatment: Ca/P≈1.42 (TSA_FA) and Ca/P≈1.36 (TSA_SA). Under a Ca/P ratio of 1.42, the composition was Cax(PO_4)y (amorphous calcium orthophosphate). Under a Ca/P ratio of 1.36, the composition was $Ca_8H_2(P0_4)_6$' $5H_2O$ (octacalcium orthophosphate). NaOH treatment was also shown to significantly improve the bioactivity of the Ti surfaces by creating a mesoporous surface topography conducive to cell responses.[26]

TSA_SA group has a higher E*corr* than the T and TSA_S groups, indicating excellent corrosion resistance. The I*corr* of TSA_FA and TSA_SA were significantly higher than those of the T group. Note that the calculation of the corrosion current is based on the actual surface exposed area. As can be seen from the surface structure in Fig. 1, the surface area in the T group is much smaller than the surface area in

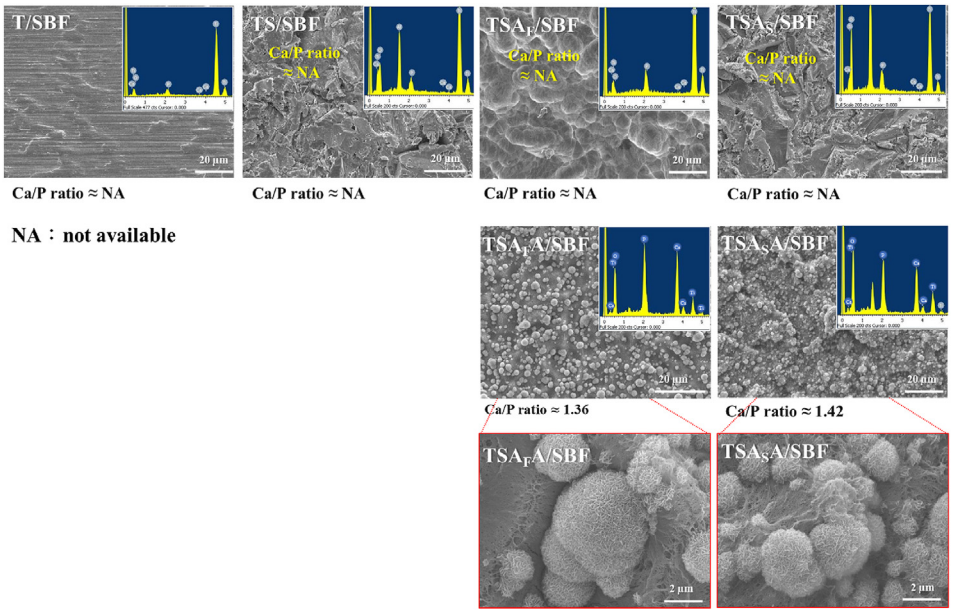

Figure 10 Bioactivity of all samples in simulated body fluid as indicated by apatite formation. T: grade 4 Ti; TS: T discs underwent sandblasting; TSA_F: the TS disks were etched in an acid bath of HNO_3/HF; TSA_S: the TS disks were etched in an acid bath of HCl/H_2SO_4; TSA, TSA_FA and TSA_SA: the TS, TSA_F, and TSA_S samples were soaked in NaOH.

the NaOH treatment group. The I*pass* of TSA_S and TSA_SA were higher than those of T, whereas the values of TSA_SA were higher than those of TSA_S. This means that the observed increase in I*pass* can be attributed to the alkaline treatment process.

Based on FE-SEM/FIB data, we determined that the surfaces of samples treated with NaOH solution possessed a 3D porous surface, which greatly increased the surface area. Taken together, we can infer that the actual I*corr* and I*pass* values on sample surfaces were lower than the measured values.

Note that high E*corr* and low I*corr* and I*pass* values indicate high resistance to corrosion.[8,9] It appears that the oxide layer significantly increased the corrosion resistance of the Ti alloy in SBP. Table 1 compares the results in the current study with those in previous reports. The E*corr* values of TSA_F samples in SBP were higher than those in other groups. The I*corr* value of TSA_F in SBP was lower than that of T samples, and the I*corr* of TSA_SA was twice that of T samples; however, the I*corr* values of TSA_F and TSA_S were lower than those of T samples. This means that acid-etching treatment actually decreased susceptibility to corrosion. The decrease in I*corr* values can be attributed to the alkaline treatment process, which increased the surface area of the samples (Fig. 1), which had a corresponding effect on current density. The high corrosion resistance of TSA_FA samples can be attributed to the protective surface oxide film composed mainly of TiO_2. Note that the specific role of TiO_2 in corrosion resistance can be attributed to the formation of anatase TiO_2 (Fig. 4).[27] Taken together, the FE-SEM (Fig. 1), XPS (Fig. 3), XRD (Fig. 4), and potentiodynamic polarization curves (Fig. 5 and Table 1) clearly demonstrated that the porous oxide layer enhanced corrosion resistance.

FE-SEM micrographs show that hMSC cells incubated on NaOH-treated samples have excellent adhesion between the cells and the substrate (Fig. 7). Under higher magnification levels, the TSA_FA and TSA_SA samples both presented distinct nanopores, as shown in Fig. 1. Cross-sectional images revealed that the pores were interconnected. As shown in Figs. 3 and 4, the nanoporous material comprised three types of Ti oxide, including anatase-TiO_2, Ti_3O_5, and Ti_2O_3. Many studies have demonstrated that Ti oxides can improve corrosion resistance and protect cells from the effects of potentially corrosive environments.[28]

Biological response tests revealed that alkaline etching had a more profound effect on biocompatibility than did sandblasting/acid etching. Previous *in vitro* studies reported that surface roughness of 250 nm - 1.5 μm can promote cellular activity.[29] hMSCs cultures in the current study revealed that roughening the surfaces enhanced cell attachment and proliferation *in vitro* (Figs. 7 and 8). A few studies have emphasized that cell growth depends on the ability of nanoscale proteins to enter nanopores on titanium surface,[17] and the findings in the current study support this assertion.

Based on the observation of cell growth from the 1—5 day, it can be seen that the growth of cells on samples treated with NaOH is better than that on samples without NaOH treatment (Fig. 8). Enhanced cell proliferation can be attributed to an increase in nascent cell adhesion facilitated by the nanoporous surface (Fig. 7). As shown in Figs. 7 and 8, our cell adhesion results corresponded to cell proliferation results in the current study. They also corresponded to cell adhesion results in previous studies.[22,24,26,30]

The nanoporous oxide layers that formed on the TSA_FA and TSA_SA samples presented an average lateral mesh size of roughly 70—100 nm (Figs. 1 and 2), which is well within

the ideal parameters for the aggregation and activation of cell adhesion-related integrins (50—100 nm) mentioned in previous studies.[30] Engineering nanoscale features on Ti implant surfaces can enhance osseointegration by promoting cell adhesion and inducing changes in growth behavior.[31] The nanopores in the current study were shown to have positive effects on cell adhesion and spreading (Fig. 7). The most important factor in promoting osteogenic responses is the size of surface structures. Nano-scale structures enhance cell proliferation, regardless of the architecture (fibrous, porous, or cylindrical).[32]

Alizarin Red S staining is a qualitative indication of mineralized calcium deposits on the surface of a material. As shown in Fig. 9, cell mineralization in the acid-treated group was more pronounced than in the untreated sample at days 7 and 14. In addition, the color of alizarin red staining is more pronounced on alkaline-treated samples. We believe that this is due to the deposition of calcium in the nanopores during the CPC treatment and the calcium ions in the pores that have penetrated the nanopores. CPC cannot completely dissolve the calcium ions inside the pores. The quantitative and qualitative results show slight differences.

As shown in Fig. 8, our objective in this study was to promote cell growth by optimizing existing surface modification techniques to create a 3D structural environment that mimics the cellular matrix. We also sought to promote the corrosion resistance of Ti under physiological conditions. The facile surface treatment scheme developed in this study produces Ti surface with outstanding physical and chemical properties as well as good biological responses.

This paper presents a facile approach to the treatment of Ti implants involving the formation of a bio-functional porous surface coating with structures at the nano-to sub-micro scale. The proposed coating comprises a porous (biocompatible) TiO_2 outer layer and a dense (protective) TiO_2 inner layer. The oxide layer with an ECM-like structure (anatase-TiO_2) was shown to enhance resistance to corrosion, as demonstrated by an increase in corrosion potential as well as decreases in corrosion rate and passive current in SBP. The porous oxide layer was also shown to enhance the bioactivity and cell responses (adhesion, proliferation, and mineralization) of hMSCs. The proposed surface treatment method has considerable development potential for the fabrication of dental and orthopedic implants.

Declaration of competing interest

The authors have declared that there are no competing interests.

Acknowledgments

This research was funded by the National Science and Technology Council (No. 112-2221-E-038-006-MY3), Wan Fang Hospital-Taipei Medical University Program (111 TMU-WFH-20; 112 TMU-WFH-26) and the National Taiwan University of Science and Technology-Taipei Medical University Joint Research Program (No. NTUST-TMU-112-02; No. 112-TMU-NTUST-112-02).

The authors also thank Mr. Sheng-Chung Liao of the Instrument Center at the National Taiwan University of Science and Technology for the FE-SEM.

References

1. Revathi A, Borrás AD, Muñoz AI, Richard C, Manivasagam G. Degradation mechanisms and future challenges of titanium and its alloys for dental implant applications in oral environment. *Mater Sci Eng C C* 2017;76:1354—68.
2. Golvano I, Garcia I, Conde A, Tato W, Aginagalde A. Influence of fluoride content and pH on corrosion and tribocorrosion behaviour of Ti13Nb13Zr alloy in oral environment. *J Mech Behav Biomed Mater* 2015;49:186—96.
3. Gaur S, Agnihotri R, Albin S. Bio-tribocorrosion of titanium dental implants and its toxicological implications: a scoping review. *Sci World J* 2022:4498613.
4. Dos Santos VM. Titanium pigment and yellow nail syndrome. *Skin Appendage Disord* 2016;1:197.
5. Kirmanidou Y, Sidira M, Bakopoulou A, et al. Assessment of cytotoxicity and antibacterial effects of silver nanoparticle-doped titanium alloy surfaces. *Dent Mater* 2019;35:e220—33.
6. Epsley S, Tadros S, Farid A, Kargilis D, Mehta S, Rajapakse CS. The effect of inflammation on bone. *Front Physiol* 2021;11:511799.
7. Asa'ad F, Thomsen P, Kunrath MF. The role of titanium particles and ions in the pathogenesis of peri-implantitis. *J Bone Metab* 2022;29:145.
8. Bocchetta P, Chen LY, Tardelli JD, Reis AC, Almeraya-Calderón F, Leo P. Passive layers and corrosion resistance of biomedical Ti-6Al-4V and β-Ti alloys. *Coatings* 2021;11:487.
9. Nascimento CB, Donatus U, Ríos CT, Oliveira MC, Antunes RA. A review on corrosion of high entropy alloys: exploring the interplay between corrosion properties, alloy composition, passive film stability and materials selection. *Mater Res-Ibero-am J Mater* 2022;25:e20210442.
10. Sarker A, Leary M, Fox K. Metallic additive manufacturing for bone-interfacing implants. *Biointerphases* 2020;15:050801.
11. Borcherding K, Schmidmaier G, Hofmann GO, Wildemann B. The rationale behind implant coatings to promote osteointegration, bone healing or regeneration. *Injury* 2021;52:S106—11.
12. Katsuura Y, Wright-Chisem J, Wright-Chisem A, Virk S, McAnany S. The importance of surface technology in spinal fusion. *HSS J* 2020;16:113—6.
13. Rani VD, Vinoth-Kumar L, Anitha VC, Manzoor K, Deepthy M, Shantikumar VN. Osteointegration of titanium implant is sensitive to specific nanostructure morphology. *Acta Biomater* 2012;8:1976—89.
14. Wei Y, Zhang Q, Thompson JE. The wetting behavior of fresh and aged soot studied through contact angle measurements. *ACS* 2017;7:11.
15. Li Q, Yang L, Wang Z, Zhang H, Liu Z, Chen Q. The superior properties of CrN coatings prepared by high power pulsed reactive magnetron sputtering. *AIP Adv* 2020;10:015125.
16. Cai S, Wu C, Yang W, Liang W, Yu H, Liu L. Recent advance in surface modification for regulating cell adhesion and behaviors. *Nanotechnol Rev* 2020;9:971—89.
17. Janmohammadi M, Nourbakhsh MS, Bahraminasab M, Tayebi L. Effect of pore characteristics and alkali treatment on the physicochemical and biological properties of a 3D-printed polycaprolactone bone scaffold. *ACS Omega* 2023;8:7378—94.
18. Hakkinen KM, Harunaga JS, Doyle AD, Yamada KM. Direct comparisons of the morphology, migration, cell adhesions, and actin cytoskeleton of fibroblasts in four different three-dimensional extracellular matrices. *Tissue Eng* 2011;17:713—24.

19. Borciani G, Montalbano G, Baldini N, Cerqueni G, Vitale-Brovarone C, Ciapetti G. Co-culture systems of osteoblasts and osteoclasts: simulating in vitro bone remodeling in regenerative approaches. *Acta Biomater* 2020;108:22—45.
20. Benea L, Simionescu-Bogatu N. Reactivity and corrosion behaviors of Ti6Al4V alloy implant biomaterial under metabolic perturbation conditions in physiological solutions. *Materials* 2021;14:7404.
21. Gill P, Musaramthota V, Munroe N, et al. Surface modification of Ni-Ti alloys for stent application after magneto-electropolishing. *Mater Sci Eng C* 2015;50:37—44.
22. Rodrigues AV, Oliveira NT, dos Santos ML, Guastaldi AC. Electrochemical behavior and corrosion resistance of Ti-15Mo alloy in naturally-aerated solutions, containing chloride and fluoride ions. *J Mater Sci Mater Med* 2015;26:5323.
23. Lukaszewska-Kuska M, Wirstlein P, Majchrowski R, Dorocka-Bobkowska B. The effects of titanium topography and chemical composition on human osteoblast cell. *Physiol Res* 2021;70: 413—23.
24. Das R, Ambardekar V, Pratim Bandyopadhyay P. *Titanium dioxide and its applications in mechanical, electrical, optical, and biomedical fields*, 7. London, UK: IntechOpen, 2022.
25. Voltrova B, Hybasek V, Blahnova V, et al. Different diameters of titanium dioxide nanotubes modulate Saos-2 osteoblast-like cell adhesion and osteogenic differentiation and nano-mechanical properties of the surface. *RSC Adv* 2019;9: 11341—55.
26. Staufert S, Torlakcik H, Pane S, Hierold C. Highly adherent parylene-C coatings with nanostructuring for enhanced cell adhesion and growth. *IEEE Trans NanoBioscience* 2019;18: 230—3.
27. Chang JH, Liu JF, Sun YS, Wu CP, Huang HH, Han Y. Mesoporous surface topography promotes bone cell differentiation on low elastic modulus Ti—25Nb—25Zr alloys for bone implant applications. *J Alloys Compd* 2017;707:220—6.
28. Pan Y, Guan WM. Origin of enhanced corrosion resistance of Ag and Au doped anatase TiO2. *Int J Hydrogen Energy* 2019;44: 10407—14.
29. Luo J, Walker M, Xiao Y, Donnelly H, Dalby MJ, Salmeron-Sanchez M. The influence of nanotopography on cell behaviour through interactions with the extracellular matrix - a review. *Bioact Mater* 2021;15:145—59.
30. Yu J, Huang J, Jansen JA, Xiong C, Walboomers XF. Mechano-chemical mechanism of integrin clustering modulated by nanoscale ligand spacing and rigidity of extracellular substrates. *J Mech Behav Biomed Mater* 2017;72:29—37.
31. Cerqueira A, Romero-Gavilán F, García-Arnáez I, et al. Characterization of magnesium doped sol-gel biomaterial for bone tissue regeneration: the effect of Mg ion in protein adsorption. *Mater Sci Eng C* 2021;125:112114.
32. Nuhn H, Blanco CE, Desai TA. Nanoengineered stent surface to reduce in-stent restenosis in vivo. *ACS Appl Mater Interfaces* 2017;9:19677—86.